ADVANCED MATERIALS
www.advmat.de

Dendrite-Free Lithium Deposition Induced by Uniformly Distributed Lithium-Ions for Efficient Lithium Metal Batteries

*Xin-Bing Cheng, Ting-Zheng Hou, Rui Zhang, Hong-Jie Peng, Chen-Zi Zhao, Jia-Qi Huang, and Qiang Zhang**

Rechargeable lithium (Li) metal-based batteries (LMBs) have been extensively investigated for electrochemical energy storage devices. The high-energy-density of Li metal anode has fueled potential applications of LMBs in portable electronics, electric vehicles, and most recently in aerospace fields.[1–3] However, uncontrolled dendritic lithium growth that is inherent in these batteries (upon repeated charge/discharge cycling) has prevented their practical applications over the past 40 years.[4] In the 1990s, Li-ion batteries (LIBs) were designed to remedy the dendrite problem by hosting Li in a graphitic electrode, leading to tremendous success of LIBs in the portable electronic and electric vehicle markets.[5] However, the dendrite issue of Li metal is still a critical challenge, especially for the high-rate LIBs in transportation applications. Because of the small potential difference between Li ion insertion and plating, a working LIB can be easily transformed to a LMB by too rapid charging, operating it at very low temperature, or by overcharging the battery. Consequently, inhibiting dendrite growth is not only the first step to the commercialization of high-energy-density LMBs (such as Li-sulfur (S) and Li-oxygen batteries), but also a significant improvement in the safety for current LIBs.

Li dendrite is referred to a branched or tree-like structure of Li metal depositing on the anode surface. To protect Li metal, it is rewarding to modify the solid electrolyte interphase (SEI), which is formed from the spontaneous reactions between Li metal and electrolyte.[6,7] The use of various electrolyte additives, including lithium bis(trifluoromethanesulfonyl)imide (LiFSI),[8–10] halogenated salt,[11] 1,1,2,2-tetrafluoroethyl-2,2,3,3 tetrafluoropropylether,[12] trace-amount of H_2O,[7] Cs^+ ions,[13,14] and concentrated electrolyte,[10,15] are considered to enhance the stability and uniformity of the SEI layer. Nevertheless in most cases, the formed SEI layer in organic electrolyte has a low modulus and fails to withstand the mechanical deformation induced by the dendrite growth. The incomplete SEI layer cannot provide a continuous and effective protection for the Li deposits, rendering LMBs a low Coulombic efficiency and poor lifespan. Consequently after the intrinsic and inevitable Li dendrite nucleation, the most pivotal issue is to inhibit the continuous growth of large dendrites, avoid the dendrite penetration through the separator, and maintain a safe and efficient Li metal anode.

Compared with the attempts to construct the compact SEI layer and to prevent the penetration of Li dendrites by a strong mechanical barrier, preventing self-amplified growth of the dendrites is also considered. Zhang and co-workers conducted a pioneer exploration on inhibiting the dendrite growth through Cs^+ assistant.[13] The Cs^+ ions are applied to force further deposition of Li to adjacent regions of the anode rather than the initial growth tip of the Li protuberances. Consequently, large dendrite growth is eliminated. Hoffmann and co-workers demonstrated that pulse charging can significantly reduce the average dendrite length by 70% relative to direct current charging.[16a] Moreover, the 3D conductive matrix is another effective strategy to self-limit the size of Li deposits less than the nanostructured current collector and improve the Coulombic efficiency to 95%.[17] Archer and co-workers employed nanostructured electrolyte with good toughness, high mechanical modulus, high ionic conductivity, and low interfacial impedances at room temperature to inhibit the dendrite growth.[2,3,18–20] Those strategies have presented a totally novel perspective to inhibit the large dendrite growth, where the interaction between Li ions and the current collector is mainly guided by the physical principles such as electrostatic force. The fact that how Li ions interact with the substrates plays a crucial role in their deposition behaviors.

Besides the modulation on physical interaction, chemical force is another key aspect in the interaction of matter. For example, the surface chemistry has received considerable attention and achieved great success in the fields of Li-S batteries, where in usual cases, sulfur dissolves and deposits repeatedly toward unstable performance.[21] Since Li dendrite growth originates mainly from the spatial inhomogeneity in Li ion distribution on the entire electrode surface, it will significantly contribute to dendrite-inhibition behavior of Li metal anode if one material can realize the even distribution of Li ions on the electrode surface. Inspired by the similar chemical route to stabilize S cathodes, a stable Li metal anode may benefit from the enhanced chemical affinity of Li ions to the chosen material.

In this contribution, 3D glass fiber (GF) cloths (Figure S1, Supporting Information) with large quantities of polar functional groups (Si—O, O—H, O—B) are employed to realize a dendrite-free Li metal anode (**Figure 1**). SiO_2 is the major gradient of GF cloth, which is an important additive in the polymer electrolyte to improve the conductivity to inhibit the dendrite growth.[3,19,22] SiO_2 (or GF cloth) herein is employed to uniformly distribute Li ions on the conventional 2D Cu

X.-B. Cheng, T.-Z. Hou, R. Zhang, H.-J. Peng, C.-Z. Zhao, Prof. J.-Q. Huang, Prof. Q. Zhang
Beijing Key Laboratory of Green Chemical Reaction Engineering and Technology
Department of Chemical Engineering
Tsinghua University
Beijing 100084, China
E-mail: zhang-qiang@mails.tsinghua.edu.cn

DOI: 10.1002/adma.201506124

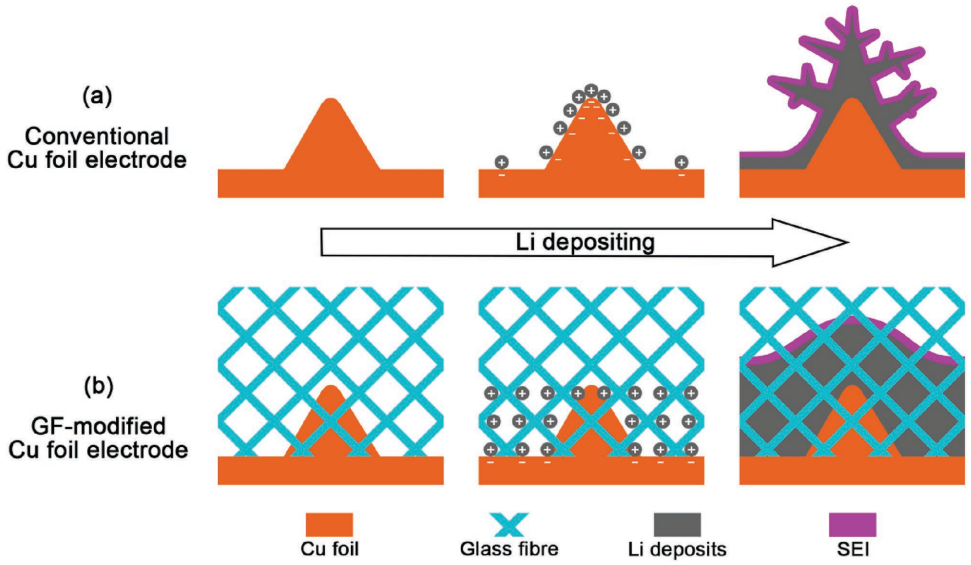

Figure 1. Schematic diagrams of Li deposition. a) The routine 2D Cu foil electrode is always with an uneven surface that induces inhomogeneous electron distribution. Li ions aggregate near the protuberance on the 2D surface with a stronger field strength than the flat during continuous Li depositing. The agminated Li ions can trigger Li dendrite growth. b) GF cloth is with large quantities of polar functional groups (Si—O, O—H, O—B), resulting in a strong interaction with Li ions. The concentrated Li ions by the protuberances on the Cu foil electrode are evenly redistributed, therefore rendering the dendrite-free Li deposits.

foil current collector to obtain the dendrite-free Li deposits on Li metal anode. The deposition behavior of Li ions were investigated by both theoretical calculation, electrochemical performance evaluation, and detailed structural analysis. The deposition of Li onto Cu foils was selected as control sample in this work.

Cu foils are widely accepted as current collectors for Li metal anode. However, due to the uneven surface of Cu foils, there are large protuberances on the electrode surface, further inducing nonuniform distribution of electric field near the Cu surface during charging and finally leading to the inhomogeneous charge distribution. Li ions are easily adsorbed on the tips of the protuberances of Cu foils due to the large electric field intensity, which is commonly known as the "tip effect."[23] The locally high electric field and concentrated Li ions expedite the nucleation and growth of Li metal at the local point, which gradually evolves into Li dendrites. These dendrites increase the surface roughness and strengthen the tip electric field intensity, triggering continuous growth of tree-like large dendrites. Therefore, the dendrite issue of Li metal anode is self-amplified as the result of such a ripple effect (Figure 1a). When GFs with a diameter of 10 μm are introduced on the anode surface, the polar functional groups on the surface of GFs can adsorb considerable Li ions to compensate the electrostatic interactions between Li ions and protuberances,[24] avoiding the accumulation of Li ions around protuberances. The Li ions tend to evenly redistribute within the GF frameworks. Because the GF is nonconductive, the Li ions can only epitaxially grow from former Li layer. Consequently, the ripple effect is terminated and a dendrite-free morphology of Li deposits is achieved (Figure 1b).

The strong interaction between Li ions and GFs is considered as the key to inhibiting dendrite formation. Fourier transform infrared spectrometry (FTIR) was applied to explore functional groups in GF and probe the specific intermolecular interactions. As illustrated in **Figure 2**a, the spectrum of GF exhibits typical SiO_2 absorbance peaks of Si—O—Si around 1113–965 cm^{-1} and O—Si—O at 793 cm^{-1}. The weak absorbance peaks at 3424 and 1384 cm^{-1} are assigned to O—H bond of the absorbed water and O—B—O bond of B_2O_3 impurities, respectively.[25] The functional groups of high polarities (Si—O, O—H, and O—B) in the chemically stable GF cloth enhance the interactions between Li ions and GF.

To demonstrate the interaction between Li ions and GFs at the macroscopic vision, the contact angle test was conducted by dropping the electrolyte (1.0 mol L^{-1} lithium bis(trifluoromethane-sulfonyl)imide-1,3-dioxolane/1,2-dimethoxyethane, LiTFSI-DOL/DME) vertically onto a Cu foil and a GF cloth (Figure 2b). The contact angle of electrolyte droplet on the Cu foil surface is 34°, indicating the moderate hydrophilicity of Cu foil. However, GF exhibits an even better hydrophilicity with a contact angle of nearly 0°, indicating that electrolyte droplets can completely penetrate into the GF cloth. Compared with other less polarized materials, GF cloth renders a better wetting state for polarized molecules of electrolyte. The enhanced affinity with electrolyte affords the large holdup of electrolyte in the GF matrix, thus decreasing the Li ion concentration gradient before Li ions reach the electrode surface.

The nanoscale interfacial interaction between Li ions and GFs/Cu foil was further verified from a computational perspective. PW91 level calculations based on density functional theory were conducted to obtain the adsorption geometries and energies of Li atom(s) on different substrates, where GF was modeled as quartz SiO_2 (110) surface while an infinite (111) surface of Cu to simulate the exposed surface of Cu foil. A Cu (221) surface model was also considered to mimic the steps on Cu (111) face where deposition is more likely to occur. Figure 2c exhibits the binding energies (E_b) of Li atom(s) on SiO_2 (110) surface, (111) plane of Cu, and step site on Cu (111).

Adv. Mater. **2016**,
DOI: 10.1002/adma.201506124

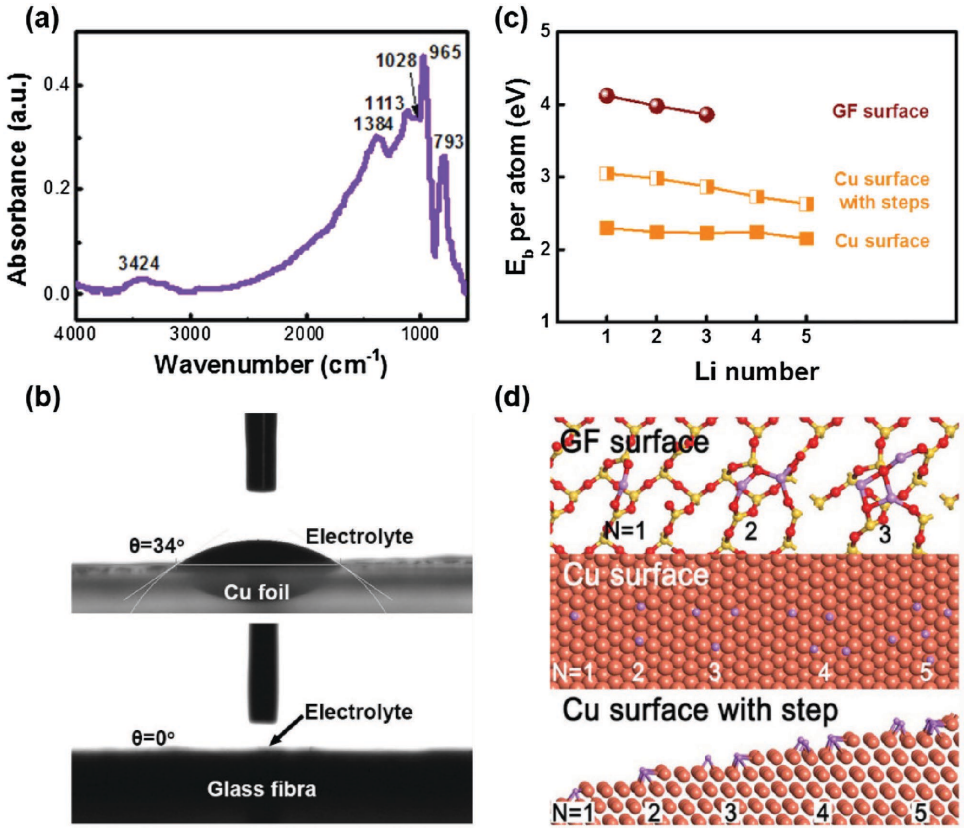

Figure 2. Verifying the attraction forces between the polar functional groups of GF and Li ions in the electrolyte. a) FTIR spectrogram of GF. b) Contact angles of LiTFSI-DOL/DME electrolyte on the Cu foil and GF. c) Binding energy (E_b) per Li atom of different types of surface and Li numbers. d) Configurations of different numbers (N) of Li atoms that bind to the three surfaces. The copper, silicon, oxygen, and lithium atoms are denoted as spheres in orange, yellow, red, and purple, respectively.

The difference of their affinity is noteworthy. Cu, which shares some similar properties with Li as metal, only provides a limited binding energy of 2.23 eV in average. The Li affinity of Li atom at the Cu step site is a little stronger with additional binding energy of 0.62 eV. However, impressively, an elevated binding energy of 3.99 eV is generated between SiO_2 and Li. As shown in Figure 2d, their configuration geometries are prominently different, which well interprets their differences in E_b. All the three surfaces can adsorb Li atoms without agglomerating together. On the Cu surface, Li atoms form weak metallic bond with lower binding energy, even in the step model. On the SiO_2 surface, Li atoms form electrovalent bonds with the surface terminal O atoms that is single-bonded before. The strong interaction between Li and O manifests a strong driving force for Li ions to be strongly absorbed by GF cloth.

To prove the uniformly distributed Li ions near the protuberances of 2D Cu foil, a calculation of finite element method (FEM) was conducted (Figure S2, Supporting Information). The calculation results of FEM simulation for Li ion distribution on the Cu foil anode with and without GF cloth are shown in Figure S2b,c (Supporting Information). Due to the strong interactions between GF framework and Li ions demonstrated in Figure 2, the concentrated Li ions near the protuberances of conventional Cu foil anode are uniformly redistributed. Consequently, Li ion distribution near Cu foil surface with GF cloth is much more uniform than that without GF cloth. The evenly distributed Li ions will finally render the dendrite-free morphology.

The anode morphology was monitored by the scanning electron microscopy (SEM) (**Figure 3**). There are large amounts of visible Li dendrites and dead Li on the surface of routine Li metal anode after Li depositing (Figure 3a). The top surface of the as-deposited Li exhibits a nonuniform structure with long Li filaments (Figure 3b). The tree-like large dendrites have a diameter of around 5 μm and a length of 20–40 μm (Figure 3c). These large dendrites not only induce huge safety risk, but also cause poor efficiency of LMBs. In contrast to the routine dendritic morphology, GF modified Li electrode displays a dendrite-free morphology. Li is sandwiched between the Cu foil substrate and the GF matrix at a low lithiation capacity of 0.5 mAh cm^{-2} (Figure 3d–f). GFs assist to homogeneously redistribute the Li ions that accumulate around the protuberances on the Cu foil. Driven by the thermodynamics of electroplating, Li deposits uniformly as a result of homogeneous distribution of Li ions. As the lithiation capacity increases to 2.0 mAh cm^{-2}, Li further grows and fills in the GF cloth. The sandwiched layer becomes thicker as well. The top surface of the sandwiched Li layer exhibits a crisscross pattern which is replicated from the interpenetrated network-like morphology of the GF cloth (Figure 3g). However, no dendrite can

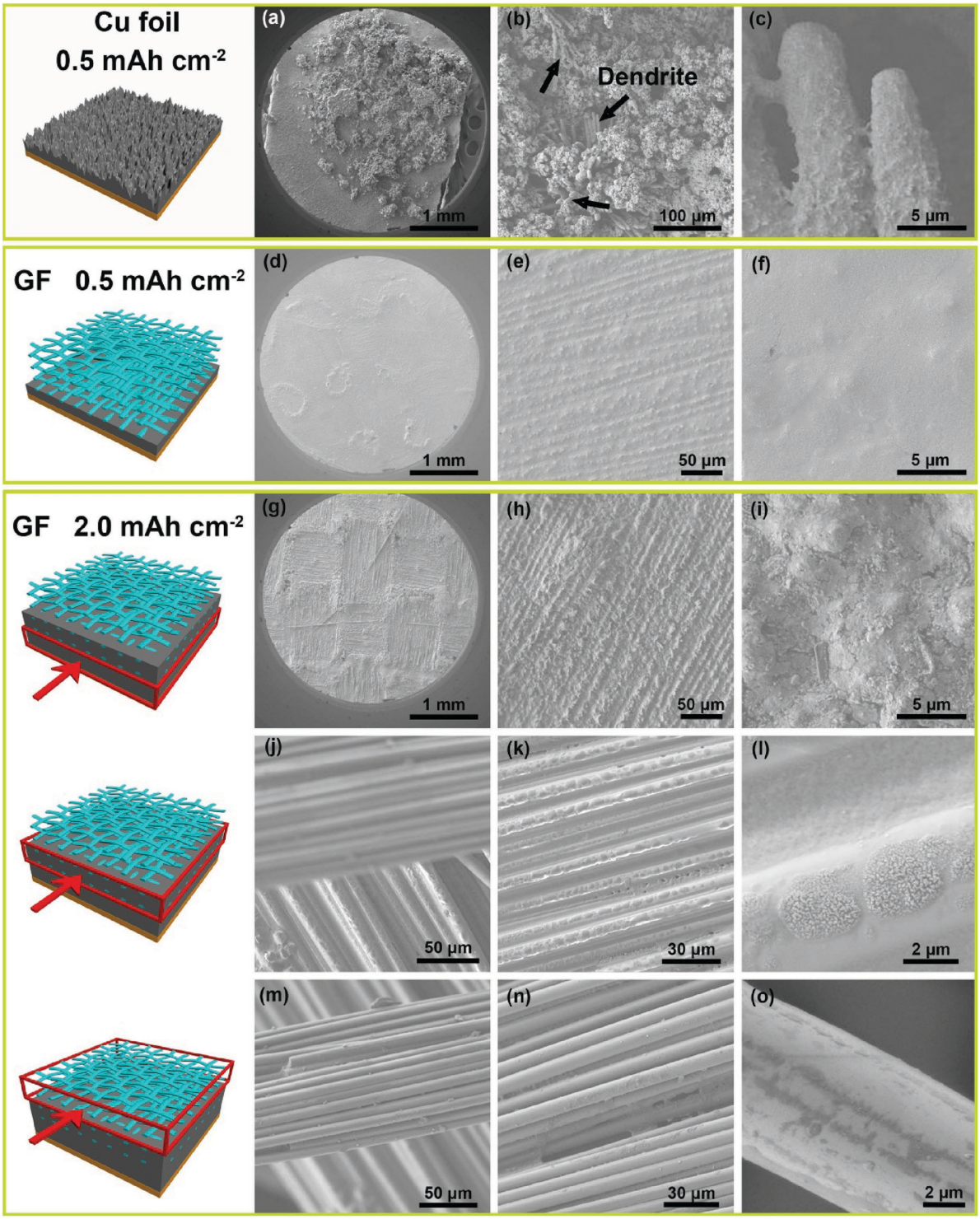

Figure 3. SEM images of the morphologies after Li deposits on Cu substrates at a current density of 0.5 mA cm^{-2} for different lithiation capacities. SEM images of Li deposits for 0.5 mAh cm^{-2} on a–c) routine Cu substrates and d–f) GF modified Cu substrates. SEM images of Li deposits for 2.0 mAh cm^{-2} on the GF modified Cu substrates from the g–i) bottom, j–l) middle to m–o) top layer.

be observed (Figure 3h,i). During the further deposition of Li within the GF cloth, Li grows epitaxially from the underneath sandwiched layer and upon the surface of each GF. Therefore, Li is embedded into the interspace of the GF matrix while no dendrite forms (Figure 3j–l). Due to low electrical conductivity of GFs, the Li layer becomes thicker from the Cu foil to the sandwiched layer, and to the GF matrix. As the capacity is set to 2.0 mAh cm^{-2}, the top layer of GF is not occupied by Li and

Adv. Mater. **2016**,
DOI: 10.1002/adma.201506124

thereby acts as an isolation layer between Li deposits and the separator to maximally ensure the safety of the Li metal anode (Figure 3m–o). More importantly, no dendrite is observed protruding upward on the GF modified electrode, which is ascribed to the evenly distributed Li ions induced by the strong interaction between Li ions and GFs. The potential safety issue of LMBs can be well addressed.

GF modified Cu foil|Li cells were employed to investigate the overall electrochemical performances of the novel Li metal anodes. Coulombic efficiency is a critical index to evaluate the availability of Li in cycling. The Coulombic efficiency reported herein is calculated from the ratio of the amount of Li stripping from the Cu substrate and Li depositing in this cycle. As LiTFSI-DOL/DME electrolyte alone cannot effectively construct a stable SEI layer, $LiNO_3$ additive is introduced to enhance the SEI compactness and stability.[26,27] As explicated in **Figure 4**a, the modified electrode presents a more stable electrochemical cycling and longer service life. Under the current density of 0.5, 1.0, 2.0, 5.0, and 10.0 mA cm^{-2}, the modified cells deliver enhanced Coulombic efficiencies of 98%, 97%, 96%, 93%, and 91%, respectively. The stable cycling of the modified cells under extraordinary current density (5.0 and 10.0 mA cm^{-2}) stems from a homogeneous Li depositing and less consumption of Li and electrolyte.[28] In contrast, the cells with GF-free Cu foil current collector displays inferior electrochemical cycling performance with fluctuant Coulombic efficiencies and short service life. The GF-free Cu foil electrode can maintain a relatively high and stable Coulombic efficiency at a low rate of 0.5 mA cm^{-2}. However, when the current rate is increased to above 1.0 mA cm^{-2}, significant variation and rapid decay on the Coulombic efficiency dominate the cycling. It is well accepted that the high current rate induces the unfavorable dendrite growth of metal anodes. The resulted SEI layer is damaged and unable to prevent the Li from harsh reaction with electrolyte. But even at high current density, the nanostructured GF framework upon the Cu foil renders the Li metal anode a high Coulombic efficiency over 90%, which can efficiently suppress the depletion of the electrolyte and Li.

The charge-discharge profiles at different rates are shown in Figure 4b. The voltage hysteresis is defined as the sum of the

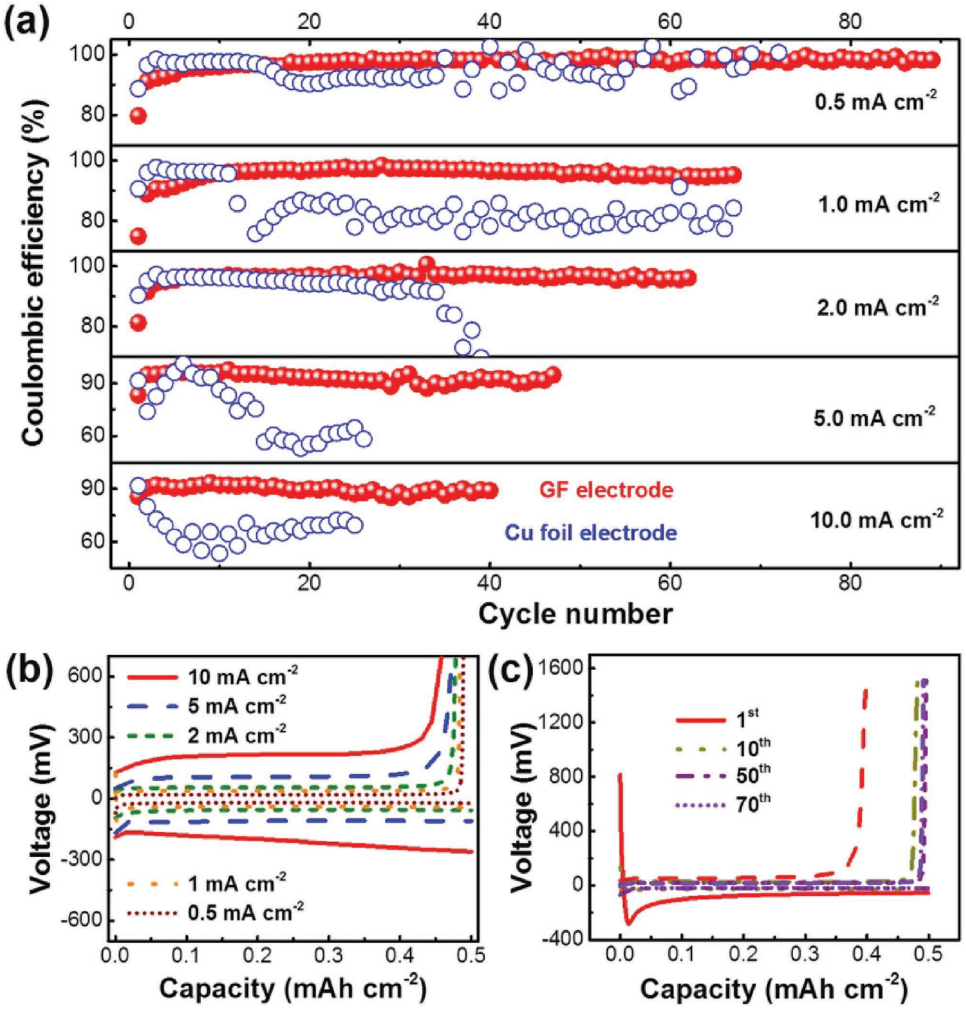

Figure 4. Electrochemical performance of GF-modified Cu substrates. a) Comparison of the Coulombic efficiency of Li deposition on bare Cu foil and GF-modified Cu foil electrode at different current densities with a lithiation capacity of 0.5 mAh cm^{-2}. The polarization of the plating/stripping for GF-modified Cu foil electrode b) at different current densities and c) at 0.5 mA cm^{-2} in different cycles.

over potential for Li depositing and Li stripping to characterize the reaction dynamics. At the current density of 0.5, 1.0, 2.0, 5.0, and 10.0 mA cm^{-2}, the modified cells manifest the voltage hysteresis of 37, 76, 99, 218, and 415 mV, respectively. Although the polarization of the cells increases with rising current density, GF modified Cu foil|Li cells with $LiNO_3$ electrolyte are stably cycled at high rates of both 5.0 and 10.0 mA cm^{-2}, maintaining Coulombic efficiencies higher than 90%. The GF modified electrode exhibits a stable polarization voltage of 37 mV upon 90 cycles at 0.5 mA cm^{-2} (Figure 4c). The stable hysteresis of modified electrode suggests the stable SEI layer, which is attributed to the uniform Li morphology induced by the GF framework. Relative to large dendrites on the Cu foil electrode, the dendrite-free morphology of the modified electrode benefits the stabilization of SEI layer upon cycling and therefore renders a superior cycling stability.

After 90 cycles of Li depositing/stripping at the current density of 1.0, 2.0, and 5.0 mA cm^{-2}, the coin cells were disassembled to collect the Li films deposited on the Cu foil for structural analysis (Figure S3, Supporting Information). With the guiding of GFs, Li ions can distribute evenly on the Cu foil surface, then uniformly deposit on the surface with dendrite-free morphology (Figure S3a,b, Supporting Information). No large dendrite can be found on the electrode after long cycling at a very high current density of 5.0 mA cm^{-2}, indicating that GF cloth with polar surface can stabilize the Li metal anode. However, there are plenty of large dendrites on the conventional Cu foil electrode. The growth of Li dendrites triggers the fracture of SEI layer. The regeneration of SEI layer inevitably consumes Li metal and electrolyte, rendering a low Coulombic efficiency and poor lifespan. The repeated consumption of Li and electrolyte, regeneration of the SEI layer, and rapid propagation of Li dendrites result in the crack of Li metal electrode (Figure S3c, Supporting Information). The width of the crack increases from 13 to 43 μm with the increase of current density from 1.0 to 5.0 mA cm^{-2}, indicating a severer destruction of the electrode structure. Dead Li derived from inhomogeneous Li stripping aggravates the low Coulombic efficiency of LMBs (Figure S3d, Supporting Information).

The cycling stability can be further verified by symmetric cell test, which is a useful method to interpret the interfacial stability and charge transfer behavior of electrochemical systems. Herein, symmetric Li+GF | GF+Li cells are assembled. Upon cycling, Li ion electrochemically deposits back and forth between the two electrodes at 1.0 mA cm^{-2}. The GF modified electrode renders a stable electrode–electrolyte interface and maintains a stable cycling performance in 500 cycles (160 h) (Figure S4, Supporting Information). A test with a lithiation capacity of 2.0 mAh cm^{-2} at a current density of 1.0 mA cm^{-2} was conducted to detect the cycling behavior. A stable cycling Coulombic efficiency of 97% is maintained (Figure S5, Supporting Information).

The superior efficiency is not only due to the dendrite-free Li deposits resulting from the uniformly distributed Li ions, but also the dense and stable SEI layer. The surface chemistry of the Cu foil anode was collected by the X-ray photoelectron spectroscopy (XPS) (Figure S6, Supporting Information). As indicated by the Li 1s, N 1s, and F 1s spectra, the SEI layer is with the same components of $ROCO_2Li$ (R = alkyl groups), LiN_xO_y, $-CF_3$, and LiF after 5th and 50th Li stripping.[26] LiN_xO_y is an important component resulting from the evolution of $LiNO_3$ additive in a working cell to stabilize the SEI layer. However, $LiNO_3$ alone cannot ensure the stable SEI layer after long cycling tests at high current rates (Figure 4a). The degeneration mechanism of the $LiNO_3$-induced SEI layer is probably because of the severe fragment of the surface layer induced by the large dendrites (Figure 3a). When GF cloth is introduced to the surface of the Cu foil anode, the uniformly distributed Li ions leads to the dendrite-free Li deposits, thus the stable SEI layer and high Coulombic efficiency are achieved after many cycles and/or at high rates. The morphology of the SEI layer on the GF cloth coating Cu foil anode is indicated by Figure S7 (Supporting Information). The as-obtained SEI layers are with conventional two-phase morphology of organic and inorganic components.[29] After 50 cycles, the SEI layer is well maintained and with the nearly same thickness. Consequently, the SEI layer formed on the Cu foil anode can be effective to improve the Coulombic efficiency in the whole life of Li metal anode, due to the synergetic effect between GF-induced dendrite-free Li deposits and $LiNO_3$ additive.

Our results demonstrate an innovative strategy to inhibit Li dendrite growth and stabilize the SEI layer to achieve both superior cycling stability and high Coulombic efficiency by placing the GF cloth between the separator and anode. The GF cloth has following outstanding characteristics on the Li metal anode:

(1) Even distribution of Li ions: The polar functional groups of GF render strong interactions between GF framework and Li ions, bringing about the even redistribution of the Li ions that have ever been concentrated by the protuberances on the Cu foil electrode. Consequently, the homogeneous distribution of Li ions affords robust dendrite-free Li depositing.
(2) High Coulombic efficiency: The dendrite-free morphology stabilizes the SEI layer without repeated consumption and reconstruction. The stable SEI layer reduces side reactions between the electrolyte and the Li metal. Consequently, the Coulombic efficiency of Li metal anode was significantly improved from 80% to 97% at 1.0 mA cm^{-2}.
(3) Enhanced safety performance: The buffer zone in the GF cloth without Li depositing under the separator further enhances the safety performance of Li metal anode at the extreme condition (high rate of 10 mA cm^{-2} and long cycling of 170 h in this work).
(4) Superior wettability with electrolyte: The enhanced affinity with electrolyte (contact angle = 0°) renders the improved holdup of electrolyte in the GF matrix, thus decreasing the Li ion concentration gradient before Li ions reach the electrode surface.

Several methods have been proposed to inhibit dendrite growth and stabilize SEI layer, including liquid electrolyte modification,[2,9,10] artificial SEI,[30] polymer and solid electrolyte,[20,31] separator coating,[32] interlayer,[33] and anode structure design.[17,34] Relative to these above-mentioned strategies, GF cloth can regulate the Li depositing and suppress Li dendrite growth at a molecular scale. Li dendrite growth is always triggered by the heterogeneous distribution of Li ions and electrons. As electron transfer is much faster than Li ion diffusion, the morphology of Li deposits relies heavily on the distribution of Li ions near the electrode surface. The uniform distribution

Adv. Mater. 2016,
DOI: 10.1002/adma.201506124

of Li ions on the Li metal surface induced by the polar functional groups of GF cloth is favorable for the dendrite-free Li depositing. Consequently, the strategy by employing the GF cloth presents an intrinsic strategy to suppress Li dendrite growth. However, the strategy is not flawless. Much more elaborate design is required to optimize the cycling performance of LMBs. As the polarization of cells cycled at high rates (5.0 and 10.0 mA cm^{-2}) is much larger, novel strategies to decrease the hysteresis of Li depositing/stripping are highly required (e.g., the use of new electrolyte with high ionic conductivity, substituting GF cloth with other similar materials).

In summary, we demonstrated a facile but effective regulation strategy to suppress Li dendrite growth by employing GFs with plenty of polar functional groups as the interlayer of Li metal anode and separator. The polar functional groups of GFs can adsorb considerable Li ions to compensate the electrostatic interactions and concentration diffusion between Li ions and protuberances of conventional Cu foil anode, avoiding the accumulation of Li ions around protuberances. The evenly distributed Li ions render the dendrite-free deposits at a high rate of 10.0 mA cm^{-2} and a high lithiation capacity 2.0 mAh cm^{-2}. Under the current density of 0.5, 1.0, 2.0, 5.0, and 10.0 mA cm^{-2}, GF-modified cells deliver enhanced Coulombic efficiencies of 98%, 97%, 96%, 93%, and 91%, respectively. By contrast, the cells with GF-free Cu foil current collector display inferior electrochemical cycling performances with fluctuant Coulombic efficiencies and short service life. Stable cycling performance of 500 cycles (170 h) is maintained for the modified electrode, demonstrating the remarkable role of GF cloth on the cycling stability of LMBs. GF-modified electrode provides a fundamental and fresh insight into the safe and highly efficient Li metal electrodes toward next-generation energy storage devices. Beyond Li metal-based batteries, the strategies to modify electrode can be grafted to other metal-containing energy-storage-systems.

Experimental Section

Materials: The Li metal counter electrode was commercially available from China Energy Lithium Co., Ltd. The GF cloth was purchased from Membrane Solutions Inc., and used as received without further treatment. The ether based electrolyte composed of LiTFSI (1.0 M) and DOL/DME with a volumetric ratio of 1:1 was purchased from Beijing Institute of Chemical Reagents. To improve the Coulombic efficiency, $LiNO_3$ additive (2.0 wt%) was introduced to the ether based electrolyte.

Structure Characterizations: The morphology of the Li deposits was characterized by a JSM 7401F SEM operated at 3.0 kV. The morphology of SEI layer on the Cu foil anode was obtained by a JEM 2100 TEM operated at 120.0 kV. FTIR spectra were collected at 423 K with 4.0 cm^{-1} resolution using a Nicolet FTIR spectrometer. The contact angle was measured by an OCA 20 Contact Angle System (Dataphysics Corp., Germany), and a 3.0 µL droplet of ether based electrolyte was used in the experiment. An Al-K_α radiation (72 W, 12 kV) at a pressure of 10^{-9} Torr was applied to achieve the X-ray photoelectron spectra. The diameter of the analyzed area was 400 µm.

Theoretical Calculation of the Interaction between Li Ions and Cu/SiO_2 Surface: The first principle calculations were conducted using spin-polarized PW91 exchange-correlation functional[35] in the framework of CASTEP[36] in Materials Studio of Accelrys Inc. A convergence criterion of 1.0×10^{-2} eV $Å^{-1}$ for the maximum final force was used for geometry optimization, and a convergence criteria of 5.0×10^{-4} Å for the maximum final displacement and 5.0×10^{-6} eV per atom for the total energy of the system was utilized for all computations. Vanderbilt-type ultrasoft pseudopotentials[37] were generated in slab calculations, and the free surfaces of Cu, Cu with step, and SiO_2 slab were separated by a 12 Å vacuum layer. The top two atom layers were allowed to fully relax with the inner layer of atom constrained. We used a $2 \times 2 \times 1$ Monkhorst–Pack mesh[38] for the sampling of the Brillouin zone, whereas valence electrons were expanded within plane wave basis set with a cut-off energy of 300 eV. The threshold for self-consistent-field density convergence was set to 2.0×10^{-6} eV per atom. Adsorption was allowed on only one side of the exposed surfaces. For quantitatively measuring the interaction between the substrates and Li_2S_4, we defined the binding energy E_b as follows

$$E_b = E(\mathrm{Sub}) + E(\mathrm{Li}) \times N - E(\mathrm{Total}) \quad (1)$$

E(Sub), E(Li), and E(Total) represent the total energies of the substrate, the Li atom, and the adsorption pair of the substrate and Li cluster, respectively. N is the number of Li atoms that bind to the surface.

The Numerical Calculation of Li Ion Distribution in a Working Cell: FEM was employed to investigate the redistribution of Li ions induced by GF framework near the surface of Cu foil. It was supposed that the Li ions deposition process was diffusion-controlled. Figure S2a (Supporting Information) exhibited the simulation model of Cu foil surface with GF framework. FEM simulation was performed in the black wireframe area with a size of 10×10 µm which was divided into a 500×500 mesh. The bottom boundary related to Cu foil uneven surface (b_1 in Figure S2a, Supporting Information) had a constant electric potential $\varphi = 0$ and a constant Li ion concentration $c = 0$ due to the diffusion-controlled assumption. The side boundaries on the surface of GF framework (b_2 in Figure S2a, Supporting Information) afforded a constant Li ion concentration $c = 0$ because of the strong interactions of Li ions and GF cloth. The top boundary related to bulk phase of electrolyte had a constant electric potential $\varphi = 100$ mV and a constant Li ion concentration $c = 1.0$ M. Other boundaries were set as Neumann boundary condition due to the mirror symmetry. The FEM iteration calculation was based on two basic equations (Equations (2) and (3))

$$\boldsymbol{W}(\boldsymbol{r},t) = -D_+ \nabla c(\boldsymbol{r},t) + \mu_+ c(\boldsymbol{r},t)\boldsymbol{E}(\boldsymbol{r}) \quad (2)$$

$$\frac{\partial c(\boldsymbol{r},t)}{\partial t} = -\nabla \cdot \boldsymbol{W}(\boldsymbol{r},t) \quad (3)$$

where t is the deposition time, r is the radius vector of each finite element, $\boldsymbol{W}(\boldsymbol{r},t)$ is the Li ion flux, $c(\boldsymbol{r},t)$ is the Li ion concentration, D_+ is the diffusion coefficient of Li ions which was set as 2.6×10^{-9} cm^2 s^{-1}, μ_+ is the mobility of Li ions which was as 1.0×10^{-7} cm^2 V^{-1} s^{-1}, $\boldsymbol{E}(\boldsymbol{r})$ is the electric field calculated by solving the Laplace equation.[39] The iteration time dt was set as 1 ms. As a comparison, the FEM simulation of Cu foil surface without GF framework was also performed by the same model, in which the b_2 boundary conditions were moved out.

Electrochemical Measurement: A two-electrode cell configuration using standard 2025 coin-type cells was employed. The two-electrode cells were assembled in an Ar-filled glove box with O_2 and H_2O content below 1.0 ppm. The Cu foil and GF cloth were punched into 13.0 mm disks as the working electrodes. A 1.0 mm thick Li metal foil was employed as the counter electrode and $LiNO_3$ (2.0%) in the LiTFSI-DOL/DME electrolyte as the electrolyte. The coin cells were monitored in galvanostatic mode within a voltage range of –0.5 to 1.5 V using Neware multichannel battery cycler. The symmetrical cells were fabricated with plate Li metal and GF as the working and counter electrodes and in the $LiNO_3$ based ether electrolyte.

Supporting Information

Supporting Information is available from the Wiley Online Library or from the author.

Acknowledgements

This work was supported by the Natural Scientific Foundation of China (21422604 and 21561130151), National Basic Research Program of China (2015CB932500), and Tsinghua University Initiative Scientific Research Program (2014z22076). T.-Z.H. and Q.Z. thank the computing time from Tsinghua National Laboratory for Information Science and Technology.

Received: December 9, 2015
Published online:

[1] L. Grande, E. Paillard, J. Hassoun, J.-B. Park, Y.-J. Lee, Y.-K. Sun, S. Passerini, B. Scrosati, *Adv. Mater.* **2015**, *27*, 784.
[2] Y. Lu, M. Tikekar, R. Mohanty, K. Hendrickson, L. Ma, L. A. Archer, *Adv. Energy Mater.* **2015**, *5*, 1402073.
[3] Z. Tu, P. Nath, Y. Lu, M. D. Tikekar, L. A. Archer, *Acc. Chem. Res.* **2015**, *48*, 2947.
[4] W. Xu, J. Wang, F. Ding, X. Chen, E. Nasybulin, Y. Zhang, J.-G. Zhang, *Energy Environ. Sci.* **2014**, *7*, 513.
[5] A. S. Arico, P. Bruce, B. Scrosati, J.-M. Tarascon, W. van Schalkwijk, *Nat. Mater.* **2005**, *4*, 366.
[6] E. Peled, *J. Electrochem. Soc.* **1979**, *126*, 2047.
[7] X.-B. Cheng, R. Zhang, C.-Z. Zhao, F. Wei, J.-G. Zhang, Q. Zhang, *Adv. Sci.* **2016**, *3*, 1500213.
[8] I. A. Shkrob, T. W. Marin, Y. Zhu, D. P. Abraham, *J. Phys. Chem. C.* **2014**, *118*, 19661.
[9] R. Miao, J. Yang, X. Feng, H. Jia, J. Wang, Y. Nuli, *J. Power Sources.* **2014**, *271*, 291.
[10] J. Qian, W. A. Henderson, W. Xu, P. Bhattacharya, M. Engelhard, O. Borodin, J.-G. Zhang, *Nat. Commun.* **2015**, *6*, 6362.
[11] Y. Lu, Z. Tu, L. A. Archer, *Nat. Mater.* **2014**, *13*, 961.
[12] C. Zu, N. Azimi, Z. Zhang, A. Manthiram, *J. Mater. Chem. A.* **2015**, *3*, 14864.
[13] F. Ding, W. Xu, G. L. Graff, J. Zhang, M. L. Sushko, X. L. Chen, Y. Y. Shao, M. H. Engelhard, Z. M. Nie, J. Xiao, X. J. Liu, P. V. Sushko, J. Liu, J. G. Zhang, *J. Am. Chem. Soc.* **2013**, *135*, 4450.
[14] Y. Zhang, J. Qian, W. Xu, S. M. Russell, X. Chen, E. Nasybulin, P. Bhattacharya, M. H. Engelhard, D. Mei, R. Cao, F. Ding, A. V. Cresce, K. Xu, J.-G. Zhang, *Nano Lett.* **2014**, *14*, 6889.
[15] L. Suo, Y.-S. Hu, H. Li, M. Armand, L. Chen, *Nat. Commun.* **2013**, *4*, 1481.
[16] a) A. Aryanfar, D. Brooks, B. V. Merinov, W. A. Goddard III, A. J. Colussi, M. R. Hoffmann, *J. Phys. Chem. Lett.* **2014**, *5*, 1721; b) M. Z. Mayers, J. W. Kaminski, T. F. Miller III, *J. Phys. Chem. C.* **2012**, *116*, 26214.
[17] a) X. B. Cheng, H. J. Peng, J. Q. Huang, F. Wei, Q. Zhang, *Small* **2014**, *10*, 4257; b) X.-B. Cheng, H.-J. Peng, J.-Q. Huang, R. Zhang, C.-Z. Zhao, Q. Zhang, *ACS Nano* **2015**, *9*, 6373.
[18] a) Z. Tu, Y. Kambe, Y. Lu, L. A. Archer, *Adv. Energy Mater.* **2014**, *4*, 1300654; b) S. Choudhury, R. Mangal, A. Agrawal, L. A. Archer, *Nat. Commun.* **2015**, *6*, 10101.
[19] a) Y. Lu, S. K. Das, S. S. Moganty, L. A. Archer, *Adv. Mater.* **2012**, *24*, 4430; b) J. L. Schaefer, D. A. Yanga, L. A. Archer, *Chem. Mater.* **2013**, *25*, 834; c) M. D. Tikekar, L. A. Archer, D. L. Koch, *J. Electrochem. Soc.* **2014**, *161*, A847.
[20] R. Khurana, J. L. Schaefer, L. A. Archer, G. W. Coates, *J. Am. Chem. Soc.* **2014**, *136*, 7395.
[21] a) H.-J. Peng, Q. Zhang, *Angew. Chem. Int. Ed.* **2015**, *54*, 11018; b) J. Song, M. L. Gordin, T. Xu, S. Chen, Z. Yu, H. Sohn, J. Lu, Y. Ren, Y. Duan, D. Wang, *Angew. Chem. Int. Ed.* **2015**, *54*, 4325; c) G. Zhou, E. Paek, G. S. Hwang, A. Manthiram, *Nat. Commun.* **2015**, *6*, 7760.
[22] S. Delacroix, F. Sauvage, M. Reynaud, M. Deschamps, S. Bruyère, M. Becuwe, D. Postel, J.-M. Tarascon, A. N. Van Nhien, *Chem. Mater.* **2015**, *27*, 7926.
[23] a) L. Enze, *J. Phys. D. Appl. Phys.* **1987**, *20*, 1609; b) L. Enze, *J. Phys. D. Appl. Phys.* **1986**, *19*, 1.
[24] a) S. Ramesh, K. H. Leen, K. Kumutha, A. K. Arof, *Spectrochim. Acta A* **2007**, *66*, 1237; b) S. Takenaka, T. Tanaka, T. Funabiki, S. Yoshida, *Faraday Trans.* **1998**, *94*, 695; c) P. Zhang, X. Li, J. Yang, S. Xu, *J. Non-Cryst. Solids* **2014**, *392–393*, 26.
[25] J.-H. Yoo, W.-K. Shin, S. M. Koo, D.-W. Kim, *J. Power Sources* **2015**, *295*, 149.
[26] a) S. Xiong, K. Xie, Y. Diao, X. Hong, *J. Power Sources* **2014**, *246*, 840; b) W. Li, H. Yao, K. Yan, G. Zheng, Z. Liang, Y.-M. Chiang, Y. Cui, *Nat. Commun.* **2015**, *6*, 7436.
[27] D. Aurbach, E. Pollak, R. Elazari, G. Salitra, C. S. Kelley, J. Affinito, *J. Electrochem. Soc.* **2009**, *156*, A694.
[28] V. Thangadurai, S. Narayanan, D. Pinzaru, *Chem. Soc. Rev.* **2014**, *43*, 4714.
[29] S. Q. Shi, P. Lu, Z. Y. Liu, Y. Qi, L. G. Hector, H. Li, S. J. Harris, *J. Am. Chem. Soc.* **2012**, *134*, 15476.
[30] a) G. Y. Zheng, S. W. Lee, Z. Liang, H. W. Lee, K. Yan, H. B. Yao, H. T. Wang, W. Y. Li, S. Chu, Y. Cui, *Nat. Nanotechnol.* **2014**, *9*, 618; b) G. Ma, Z. Wen, M. Wu, C. Shen, Q. Wang, J. Jin, X. Wu, *Chem. Commun.* **2014**, *50*, 14209; c) Y. J. Zhang, W. Wang, H. Tang, W. Q. Bai, X. Ge, X. L. Wang, C. D. Gu, J. P. Tu, *J. Power Sources.* **2015**, *277*, 304; d) E. Kazyak, K. N. Wood, N. P. Dasgupta, *Chem. Mater.* **2015**, *27*, 6457; e) Q.-C. Liu, J.-J. Xu, S. Yuan, Z.-W. Chang, D. Xu, Y.-B. Yin, L. Li, H.-X. Zhong, Y.-S. Jiang, J.-M. Yan, X.-B. Zhang, *Adv. Mater.* **2015**, *27*, 5241.
[31] a) J. Zhang, Y. Bai, X.-G. Sun, Y. Li, B. Guo, J. Chen, G. M. Veith, D. K. Hensley, M. P. Paranthaman, J. B. Goodenough, S. Dai, *Nano Lett.* **2015**, *15*, 3398; b) E. Rangasamy, Z. Liu, M. Gobet, K. Pilar, G. Sahu, W. Zhou, H. Wu, S. Greenbaum, C. Liang, *J. Am. Chem. Soc.* **2015**, *137*, 1384; c) R. Bouchet, S. Maria, R. Meziane, A. Aboulaich, L. Lienafa, J.-P. Bonnet, T. N. T. Phan, D. Bertin, D. Gigmes, D. Devaux, R. Denoyel, M. Armand, *Nat. Mater.* **2013**, *12*, 452; d) Q. Pan, D. M. Smith, H. Qi, S. Wang, C. Y. Li, *Adv. Mater.* **2015**, *27*, 5995.
[32] a) W. Luo, L. Zhou, K. Fu, Z. Yang, J. Wan, M. Manno, Y. Yao, H. Zhu, B. Yang, L. Hu, *Nano Lett.* **2015**, *15*, 6149; b) A. Ferrese, J. Newman, *J. Electrochem. Soc.* **2014**, *161*, A1350.
[33] a) Z. Liang, G. Zheng, C. Liu, N. Liu, W. Li, K. Yan, H. Yao, P.-C. Hsu, S. Chu, Y. Cui, *Nano Lett.* **2015**, *15*, 2910; b) C. Huang, J. Xiao, Y. Shao, J. Zheng, W. D. Bennett, D. Lu, L. V. Saraf, M. Engelhard, L. Ji, J. Zhang, X. Li, G. L. Graff, J. Liu, *Nat. Commun.* **2014**, *5*, 3015; c) J.-S. Kim, D. W. Kim, H. T. Jung, J. W. Choi, *Chem. Mater.* **2015**, *27*, 2780.
[34] a) J. Heine, S. Krüger, C. Hartnig, U. Wietelmann, M. Winter, P. Bieker, *Adv. Energy Mater.* **2014**, *4*, 1300815; b) X. Zhang, W. Wang, A. Wang, Y. Huang, K. Yuan, Z. Yu, J. Qiu, Y. Yang, *J. Mater. Chem. A* **2014**, *2*, 11660; c) C.-P. Yang, Y.-X. Yin, S.-F. Zhang, N.-W. Li, Y.-G. Guo, *Nat. Commun.* **2015**, *6*, 8058.
[35] J. P. Perdew, J. A. Chevary, S. H. Vosko, K. A. Jackson, M. R. Pederson, D. J. Singh, C. Fiolhais, *Phys. Rev. B* **1992**, *46*, 6671.
[36] S. J. Clark, M. D. Segall, C. J. Pickard, P. J. Hasnip, M. J. Probert, K. Refson, M. C. Payne, *Z. Kristallogr.* **2005**, *220*, 567.
[37] D. Vanderbilt, *Phys. Rev. B* **1990**, *41*, 7892.
[38] H. J. Monkhorst, J. D. Pack, *Phys. Rev. B* **1976**, *13*, 5188.
[39] J. N. Chazalviel, *Phys. Rev. A* **1990**, *42*, 7355.